The Development of Ground Impact Models for the Analysis of the Risks Associated with Unmanned Aircraft Operations Over Inhabited Areas

Paul Wu [a], Reece A. Clothier [b*]
[a] Queensland University of Technology, Brisbane, Australia
[b] Australian Research Centre for Aerospace Automation, Brisbane, Australia
* reece.clothier@rmit.edu.au

Abstract: With the emergence of Unmanned Aircraft Systems (UAS) there is a growing need for safety standards and regulatory frameworks to manage the risks associated with their operations. The primary driver for airworthiness regulations (*i.e.*, those governing the design, manufacture, maintenance and operation of UAS) are the risks presented to people in the regions overflown by the aircraft. Models characterising the nature of these risks are needed to inform the development of airworthiness regulations. The output from these models should include measures of the collective, individual and societal risk. A brief review of these measures is provided. Based on the review, it was determined that the model of the operation of an UAS over inhabited areas must be capable of describing the distribution of possible impact locations, given a failure at a particular point in the flight plan. Existing models either do not take the impact distribution into consideration, or propose complex and computationally expensive methods for its calculation. A computationally efficient approach for estimating the boundary (and in turn area) of the impact distribution for fixed wing unmanned aircraft is proposed. A series of geometric templates that approximate the impact distributions are derived using an empirical analysis of the results obtained from a 6-Degree of Freedom (6DoF) simulation. The impact distributions can be aggregated to provide impact footprint distributions for a range of generic phases of flight and missions. The maximum impact footprint areas obtained from the geometric template are shown to have a relative error of typically less than 1% compared to the areas calculated using the computationally more expensive 6DoF simulation. Computation times for the geometric models are on the order of one second or less, using a standard desktop computer. Future work includes characterising the distribution of impact locations within the footprint boundaries.

Keywords: UAS, Unmanned Aircraft Systems, Risk, Impact Distribution

1. INTRODUCTION

Unmanned Aircraft Systems (UAS) have emerged as a viable technology in numerous applications, which include surveillance, infrastructure inspection, environmental monitoring, agriculture, search and rescue and law enforcement. Like any technology, the operation of UAS has associated risks. From [1], the primary hazards associated with the operation of UAS are a:

a) collision between the Unmanned Aircraft (UA) and a Conventionally-Piloted Aircraft (CPA) situated on the ground or in the air; or
b) controlled or uncontrolled impact of the UA with terrain or objects on the terrain (*e.g.*, people or structures).

These hazards have a number of associated risks. Of primary concern are the risks to the third party people on-board CPA or people on the ground in the regions overflown, respectively. The high-level safety objective is that UAS demonstrate, as a minimum, an Equivalent Level of Safety (ELoS) to that demonstrated by CPA operations [2]. A comprehensive framework of safety regulations to manage the risks and in turn provide assurances that UAS demonstrate an ELoS has yet to be developed. In its absence National Aviation Authorities (NAAs) have imposed significant restrictions on the operation of UAS. These restrictions include limiting UAS operations to airspace segregated from all other airspace users; limiting UAS operations to uninhabited regions; or prohibiting the operation of UAS altogether. Thus, the development and promulgation of a framework of safety policy, regulations and standards to manage the risks associated with UAS operations is essential to the realisation of a sustainable civil UAS market.

Foundational to the development of justifiable safety regulations for UAS is a comprehensive understanding of the nature and level of the risks. Such an understanding is typically provided through the completion of a risk analysis [3]. For regulations relating to the operation of UAS alongside other airspace users and their integration to the existing civil airspace system (*e.g.*, rules of the air, procedures and equipage), the primary risks of concern are those associated with the hazard of a mid-air collision between an UAS and a CPA. For airworthiness regulations (*i.e.*, those primarily relating to the design, manufacture, maintenance and operation of UAS), the primary risks of concern are those that associated with a discontinuance of flight. The scope of the paper is limited to the latter of these regulatory areas. More specifically, the work presented in this paper is part of a larger program of research supporting the development of a suitable airworthiness regulatory framework for civil UAS (described in [4]). The regulatory framework described in [4] requires a top-level assessment of the risk to people on the ground across the complete spectrum of foreseeable UAS CONcepts of OPerationS (CONOPS). Such a broad and high-level assessment does not rely on detailed information on the UAS, its sub-systems, failure modes, or flight path or on the distribution of people on the ground. Such information is seldom available or practical to obtain for such a diverse range of possible systems, operations and operating environments (as illustrated in the histograms provided in [4]).

A literature review revealed an array of statistical and causal models for characterising the risk to people on the ground due to aviation activities. These include models specific to the operation of UAS (*e.g.*, [5-12]), CPA (*e.g.*, [13-20]), manned and unmanned spacecraft (*e.g.*, [21-23]) and general debris models (*e.g.*, [24]). For UAS, there is limited historical accident, incident and operational data upon which to base a meaningful statistical assessment of the safety performance of UAS operations over inhabited areas. However, a list of some notable UAS accidents are provided in [1]. Thus, the risk analysis of UAS operations over inhabited areas has relied heavily upon a number of high-level causal risk models.

The comprehensive management of the risks associated with the operation of UAS over inhabited areas requires consideration of the risks to individuals and groups [4]. A model of UAS operations over inhabited areas should therefore support the "population-based" [25] measures of: Individual Risk (IR), Collective Risk (CR) and Societal Risk (SR). However, none of the existing works identified provide assessments of all three measures. The first section of this paper (§2) summarises the different measures and, at a high-level, the different factors that need to be included in a high-level model characterising the risks of UAS operations over inhabited areas.

Key to providing an assessment of the IR and for characterising measures of SR is knowledge of the distribution of the potential impact locations of the UA given a critical failure. Traditionally, such a model has been difficult to characterise, often requiring large Monte Carlo simulations of the trajectory of the system for a particular combination of failure modes. Existing models have either made assumptions as to the nature of the distribution or have not taken it into consideration, reducing the fidelity of the measures or limiting the types of measures that can be obtained from the model, respectively. In the second section of this paper (§3), we describe the development of geometric templates that can be used to approximate the boundary and area of the impact distribution of a fixed wing aircraft under particular failure conditions. The approach uses a 6-Degree of Freedom (6DoF) model to characterise the boundary of the impact distribution, geometric "templates" are then fitted to the boundary through the use of empirical methods.

2. OVERVIEW OF METRICS

"Industry is becoming increasingly aware of the benefits of a balanced risk perspective that considers both individual and societal risk."[26] As such, the quantification of measures of IR, CR and SR and their use as the basis for expressing quantitative risk criteria is becoming commonplace in the risk management of a wide range of industries. In relation to aviation, these include the assessment and management of the risks around airports [19, 20], mid-air collisions [25, 27], and the risks due to flight test range activities (*e.g.*, [28]).

So as to ensure a comprehensive management of the risks to people over-flown, Clothier *et al.* [4] advocate the consideration of measures of IR, CR and SR in the development of airworthiness regulations for UAS. The majority of existing models (*e.g.*, [5-8, 11, 12]) characterise the risk associated with UAS operations through measures of the casualty or fatality expectation per flight hour (a measure of the CR). Models presented in [6, 9, 29] provide measures of the IR, however, none provide measures of the SR. The objective

of the following sub-sections is to briefly introduce some of the commonly used "population-based" [25] measures of CR, IR and SR and how their calculation can be related to a high-level model of the risks of UAS operations over inhabited areas.

2.1. Collective Risk

Measures of the Collective Risk (CR) are the most commonly used in the existing UAS ground risk models. CR measures describe the aggregate risk to a population of people. The measures used are the expected number of casualties or fatalities per flight hour [5-8], herein referred to as the Casualty Expectation (CE). For a given point in a UAS operation, a measure of CE can be determined from:

$$CE = \lambda \, P_{(S|F)} P_{(L|S,F)} \tag{1}$$

where:

a) $\boldsymbol{\lambda}$ is the expected number of failures per unit exposure (typically per flight hour). This is based on the assumption that failures occur continuously and independently at a constant rate $\boldsymbol{\lambda}$ (*i.e.*, failures can be described as a Poisson process). For small values of $\boldsymbol{\lambda}$, the probability of failure $\boldsymbol{P_F}$ in an interval of time $\boldsymbol{\Delta t}$ can be approximated by:

$$P_F \approx \lambda \Delta t \tag{2}$$

b) $\boldsymbol{P_{S|F}}$ is the probability that the UA strikes a person given the failure. Assuming that the UAS will impact the ground and that people are equally distributed across the area, $\boldsymbol{P_{S|F}}$ is replaced by the expected number of people struck per failure $\boldsymbol{N}$, and is given by:

$$N = \rho A_L \tag{3}$$

where, $\boldsymbol{\rho}$ is the population density and $\boldsymbol{A_L}$ is the lethal area as given in [10].

c) $\boldsymbol{P_{(L|S,F)}}$ is the probability of a level of loss (*i.e.*, casualty or fatality) given a strike. The existing models [5, 6, 9] make the conservative assumption that someone struck by an UA is killed. There are existing models characterising the probability of a casualty or fatality as a result of an impact [30-32], however incorporating these models requires consideration of the UA state (*i.e.*, position, velocity, attitude) and frangibility of the UA at the point of impact. At a high-level, $\boldsymbol{P_{(L|S,F)}}$ can also take into account the potential protection offered to those people who are sheltered within different types of structures. For example, the model specified in [5] incorporates sheltering through the inclusion of a probability of penetration factor. Modelling sheltering also requires models characterising the proportion of a population (or probability that a particular individual) resides within different types of shelters. An example of such a model is provided in [21].

2.2. Individual Risk

IR describes the risk to single exposed entities and has been defined as "the frequency at which an individual may be expected to sustain a given level of harm from the realisation of specified hazards."[33] One method for calculating the IR, referred to here as the average IR, $\boldsymbol{IR_\mu}$ is given in Eq.4.

$$IR_\mu = \frac{CE}{N} = \frac{CE}{\rho A_f} \tag{4}$$

where: $\boldsymbol{\rho}$ is the population density in the exposed area and $\boldsymbol{A_f}$ is the total area an impact can occur in, $\boldsymbol{CE}$ is the casualty expectation as given in Eq.(**1**). It is important to note that the calculation of $\boldsymbol{IR_\mu}$ is different to the concept of IR presented in [19, 34, 35], which define IR as: "the probability that an average unprotected person, permanently present at a certain location, is killed due to an accident resulting from a hazardous activity" [35] and herein referred to as the theoretical IR, $\boldsymbol{IR_T}$. Critical to the calculation of $\boldsymbol{IR_T}$ are the assumptions of an "average unprotected person"[35] and a permanent exposure to a given hazard. Based on these assumptions, $\boldsymbol{IR_T}$ essentially represents the path characteristics [36] of the phenomena causing loss. By

assuming a person is always exposed, whether they are present or not, means that $\boldsymbol{IR_T}$ is predominantly a "property of the location" [35] as opposed to the behaviour and characteristics of any one individual. In the case of the modelling of UAS operations, $\boldsymbol{IR_T}$ is primarily a function of the impact distribution of the UA and its properties on impact (*e.g.*, energy). As described by Pasman and Vrijling [37] "The IR does not change even if it is proven that nobody can be present at the moment of the accident." Clearly, the properties and assumptions underpinning $\boldsymbol{IR_\mu}$ are different to those required to determine $\boldsymbol{IR_T}$; $\boldsymbol{IR_\mu}$ is a function of the total number of people exposed, whereas $\boldsymbol{IR_T}$ is independent of the people exposed. $\boldsymbol{IR_T}$ is typically represented as iso-risk contours around a hazard source (*i.e.*, the point in the flight plan where the UAS experiences a failure). A measure of the CR can be determined from $\boldsymbol{IR_T}$ by taking into account the presence of a population. An example of this is described in Laheij *et al*. [38] and Piers [39], who describe the expected value of the potential loss of life through the integration of the spatial intersection of the distributions describing $\boldsymbol{IR_T}$ and the population density, $\boldsymbol{\rho}$.

2.3. Societal Risk

Measures of the Societal Risk (SR) [40] have gone by a number of names, for example, they have been referred to as risk profiles [41], FN-Curves [19, 42], measures of group risk [37] or catastrophic risk [28]. When used as the basis for defining safety criteria they have been referred to as: Farmer curves (after Frank Farmer who was the first to propose the use of SR metrics as safety criteria for the siting of nuclear power stations [43]) or FN-Criterion lines [42]. SR describes "the relationship between frequency and the number of people suffering from a specified level of harm in a given population from the realisation of specified hazards." [33] Ale and Piers [19] describe SR as "the chance that in a single accident in the hazard source, a certain number of victims is exceeded. It is expressed as the relationship between the number of people killed and the chance per year that this number is exceeded." Thus, SR is not a single measure but a tabularisation or graphical representation of the frequency of accidents by number of casualties (*e.g.*, injuries or fatalities).

SR can be calculated by tabularising the outcomes (*i.e.*, number of causalities or fatalities) from a complete set of scenarios. To evaluate the SR associated with the occurrence of a failure at a particular point in the flight of the UAS the complete set of potential loss scenarios needs to be evaluated and the discrete outcomes tabularised against the probability of their occurrence (*e.g.*, the potential consequence resulting from an impact at all possible impact locations). Measures of CR, including the CE, can then be determined from SR curves as described in [40, 42].

2.4. Model Requirements

Based on this brief review of existing metrics, a clear requirement has emerged: a model of the spatial distribution of the potential UA impact location given the occurrence of a failure is required. Such a model is needed to support the measurement of $\boldsymbol{IR_\mu}$ (Eq.4), to determine a measure of $\boldsymbol{IR_T}$ and to measure the SR for a failure at a given point in the operation of a UAS over an inhabited area.

Given a failure, characterising the flight trajectory from the point of failure to the impact location on the ground is dependent on a large number of factors. These factors can include: the effect of the failure on the aerodynamic performance of the UA, wind, input commands and actions of the UAS crew, terrain and the occurrence of subsequent failures. The modelling of the trajectory under failure often requires the generation of complex dynamic models (*e.g.*, kinematic models, dynamic event trees *etc*.) in order to account for all these factors. Due to the large parameter space and associated parameter uncertainties, the calculation of the impact distribution typically requires a Monte Carlo simulation (*e.g.*, an example of a Monte Carlo-based approach is provided in [21]), which can be extremely computationally expensive. As such, most of the existing models identified in the literature do not take into consideration the impact footprint [5, 7, 8, 11, 12], consequently limiting the measures of risk that can be determined from the outputs of the simulation of the model. Existing models [6, 9] have made simplifying assumptions on the boundary or distribution of impact locations. For example, [6] models the boundary of the impact distribution as the projection of an ellipse centred on the aircraft, with semi and major axes defined in relation to the glide ratio. Rather than assume a uniform probability of impact within the elliptical impact footprint boundary, [6] models the probability of

impact as a bivariate normal distribution. The approach adopted in [6], however, is computationally expensive and requires detailed information on the flight path and the nature of the terrain over-flown.

In the absence of historical data to characterise impact distributions (as is described in [20] for the modelling of public safety zones around runways at airports) or a large and complex causal model (as described in [17, 18]) there is need for an alternative and computationally efficient approach for modelling the impact distribution boundary. One such approach is explored in the next section.

3. A NOVEL IMPACT FOOTPRINT BOUNDARY MODEL

An impact footprint is needed to comprehensively characterise the spatial dependency of a person's exposure to the hazard of a UAS crash. The model is to be used to support the development of airworthiness regulations for a wide range of UAS, and as such it is assumed that detailed information on the UA and operational information including the exact flight path and hence terrain and population centres overflown, are not available. Therefore, it is not feasible to determine the impact distribution. However, for many failures, it is still possible to ascertain the boundary of the impact distribution and in turn, the area exposed to the hazard of a crashing UAS. In this section, we describe an approach for characterising the boundary of the impact footprint distribution.

A simulation of a 6DoF aircraft model is used to determine the boundary of possible ground impact locations for an UA, given a failure. The footprint boundary is generated for two case-study fixed wing aircraft: a Cessna 172 and Aerosonde UA. The 6DoF simulation is described in §3.2. A description of the 6DoF aerodynamic model is provided in [44].

The 6DoF simulation is computationally expensive to evaluate over a large number of missions and flight profiles. Further, it requires a detailed model of the aircraft, information that is not readily available for all UAS. In section §3.3, a series of geometric primitives (*i.e.*, footprint templates) are developed to approximate the footprint boundaries determined by the 6DoF simulation. In §3.4 the footprints are extrapolated to determine the aggregated footprint boundary for different phases of a flight (*e.g.*, climb/descent, cruise and loiter). The geometric footprints are computationally efficient to calculate, have a low relative error (compared to the results determined from the 6DoF model), can be determined from relatively high-level information on the UAS, and can be used to evaluate the risk for a range of mission profiles.

3.1. Applicable Failures

Not all failures have a bounded impact distribution. A bounded impact distribution is typically associated with an Unrecoverable Flight Critical Event (UFCE) [6] such as structural failures, propulsion failures, failures in flight control systems, power systems or the inadvertent activation of flight termination systems, *etc.* (*e.g.*, see Table 1.1-1 [11]). Typical emergency operating procedures often attempt to contain the UAS and its impact location to a known region by shutting down the engine or placing the aircraft into a pre-programmed descent profile. As such, these emergency procedures also have a bounded impact footprint distribution.

3.2. 6DoF Impact Footprint Boundary Model

A 6DoF aerodynamic model of the aircraft can be used to determine the maximum extents of the impact distribution (full derivation of the 6DoF model can be found in [44]) for the applicable failures described in §3.1. Using the 6DoF model, the set of possible impact points is obtained by simulating the complete set of feasible gliding descent trajectories. Specifically:

a) It is assumed that the descent trajectory comprises a turn onto a given heading angle $\boldsymbol{\phi}$ followed by a straight line glide (*i.e.*, constant flight path angle);
b) The simulation was completed for all values of $\boldsymbol{\phi}$ on $(0,2\pi)$ with the scenario of $\boldsymbol{\phi} = \mathbf{0}$ corresponding to a straight line glide (*i.e.*, no turn);

c) The simulation was completed for a range of aircraft bank angles, airspeeds, flight path angles and initial altitudes;
d) The simulation was completed for both case study aircraft (*i.e.*, Cessna 172 and Aerosonde UA).

Logically, optimal descent trajectories (*i.e.*, those with the greatest displacement from the starting point) are achieved when the aircraft flies at the minimum flight path angle (corresponding to the minimum drag velocity for the particular aircraft) and by executing a turn with a bank angle of $\boldsymbol{\mu = \pi/4}$. The maximum footprint boundary is then obtained by connecting the impact points for each of the optimal trajectories. Some example maximum footprint boundaries for the Cessna 172 are presented in Fig.1 for a range of starting altitudes.

From Fig.1, it can be seen that the footprint area grows monotonically with height Above Ground Level (AGL). At low altitudes, the footprint is shaped somewhat like a pie slice (circular sector). This is because the aircraft hits the ground before it can complete its turn (*e.g.*, Fig.1a). As altitude increases, the footprint evolves into a more rounded, almost circular shape (*e.g.*, Fig.1d). This occurs as there is sufficient height AGL such that the length of the straight-line glides is significantly larger then that of the turning circle of the aircraft. Note that the forward half of the footprint is slightly different in shape to that of the back half. In addition, the footprint shape and area varies for the different aircraft. Specifically, for the same initial conditions, the footprint area for the Aerosonde is significantly greater than that for the Cessna 172 due to the superior glide performance of the Aerosonde.

3.3 Approximating the 6DoF Footprint

The footprints determined using the 6DoF simulator (*e.g.*, Fig.1) require a detailed aerodynamic model of the aircraft. In order to calculate the impact distribution boundary for a wide range of UAS and operational profiles (*e.g.*, altitudes *etc*.), a simpler and more computationally efficient method for approximating the maximum boundary of the impact distribution is needed. This section describes the development of a set of geometric "templates" that can be used to approximate the maximum boundary of the impact distribution for fixed wing aircraft. As can be seen from Fig.1, more than one geometric template is needed to approximate the footprints achieved from different initial height AGL. Two models are determined: a high altitude model and a low altitude model. The transition altitude (*i.e.*, the height AGL at which the high altitude model provides a better approximation of the footprint boundary than that of the low altitude model) is empirically determined and is a function of the aircraft turn and glide performance.

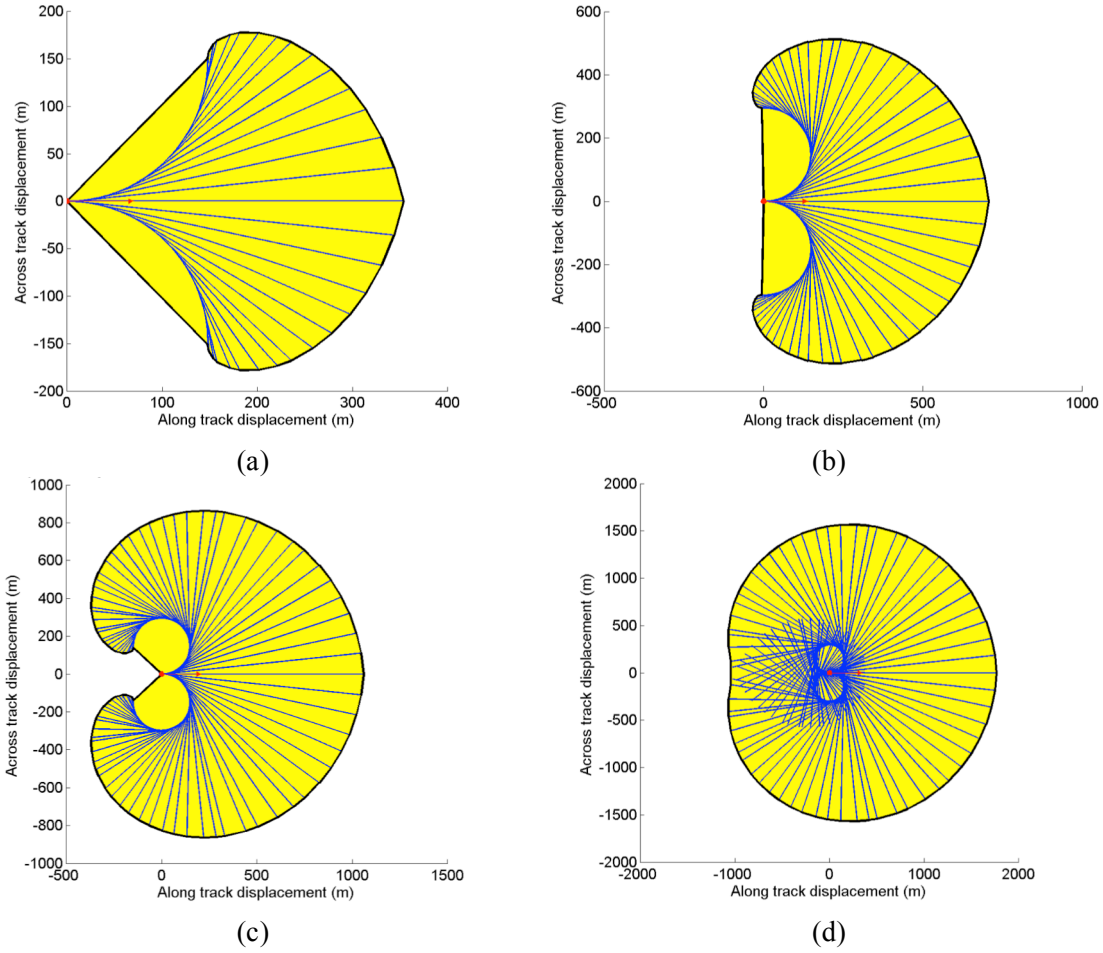

Figure 1. Impact Footprint Determined Using a Simulation of a 6DoF Model of a Cessna 172 from an Initial Height Above Ground Level of (a) 100ft, (b) 200ft, (c) 300ft and (d) 500ft.

3.3.1 High Altitude Model

A dual half-ellipse model is proposed for approximating the maximum boundary of the impact distribution at altitudes above the transition altitude. A half-ellipse is used to model the forward (positive along track) half of the footprint (with major and minor axis lengths $\boldsymbol{a_1}$ and $\boldsymbol{b_1}$ respectively). Another half-ellipse is used to model the back (negative along track) half of the footprint (with major and minor axis lengths $\boldsymbol{a_2}$ and $\boldsymbol{b_2 = b_1}$). The geometric model is illustrated in Fig.2. Note, in Fig.2 that $\boldsymbol{A}$ is the initial aircraft location, $\boldsymbol{AC}$ is the turn radius $\boldsymbol{r_t}$ for the chosen bank angle, $\boldsymbol{CD} = \boldsymbol{a_1}$, $\boldsymbol{CB} = \boldsymbol{b_1} = \boldsymbol{b_2}$, $\boldsymbol{EC} = \boldsymbol{a_2}$. $\boldsymbol{C}$ is the centre point for the forward and back ellipses.

The points $\boldsymbol{E}$, $\boldsymbol{B}$ and $\boldsymbol{D}$ are the footprint extremities in the negative $\boldsymbol{x}$ (along track), positive $\boldsymbol{y}$ (across track) and positive $\boldsymbol{x}$ directions, respectively. The parameters $\boldsymbol{a_1}$, $\boldsymbol{b_1}$ and $\boldsymbol{a_2}$ approximate the extremities of the true footprint. Both the forward and back ellipses are centred on $\boldsymbol{C}$, which is located at a distance $\boldsymbol{r_t}$ along the track from the initial point (origin) $\boldsymbol{A}$. Estimating the values of the above parameters is based on the assumption of a trajectory comprising a turn and a glide at the minimum drag velocity. This trajectory corresponds to the maximum glide distance and minimum glide path angle (and hence maximum extent of the impact distribution). The trajectory varies according to the initial starting altitude AGL. $\boldsymbol{r_t}$ is the turn radius and can be determined assuming a coordinated turn. The length of the arc traversed in this turn is a function of $\boldsymbol{r_t}$ and the turn angle $\boldsymbol{\phi}$. By using an empirically determined scalar factor of the glide path angle during the turn, it is possible to ascertain (through trigonometry) the loss in height in the execution of the turn. Using trigonometry, the remaining height AGL and flight path angle can then be used to determine the ground track distance of the glide $\boldsymbol{d_g}$. $\boldsymbol{b_1}$ can be determined as the sum of $\boldsymbol{r_t}$ and $\boldsymbol{d_g}$ for a turn angle $\boldsymbol{\phi}$ = 90° and similarly, $\boldsymbol{a_2}$ can be determined in the same manner for $\boldsymbol{\phi}$ =180°. $\boldsymbol{a_1}$ corresponds to $\boldsymbol{d_g}$ with a turn angle of $\phi = 0°$ (*i.e.* $\boldsymbol{d_g} = \boldsymbol{d_{max}}$) less $\boldsymbol{r_t}$. The area of the resultant footprint is given by:

$$A_{Dual\ Ellipse} = \frac{\pi}{2}a_1 b_1 + \frac{\pi}{2}a_2 b_1 \quad (5)$$

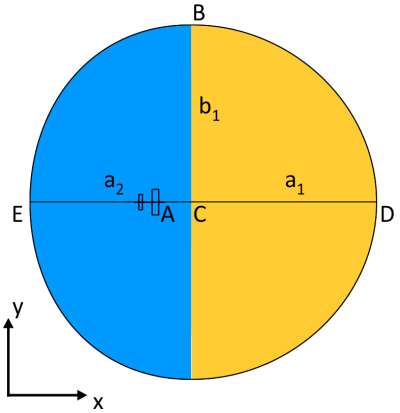

Figure 2. Geometric Primitive of the Maximum Boundary of the Impact Distribution at High Altitudes

3.3.2 Low Altitude Model

Eq.5 does not apply at lower altitudes where the air vehicle is unable to turn onto a heading angle of $\boldsymbol{\phi = 180°}$ before impacting the ground (*e.g.*, Fig.1a, Fig.1b, and Fig.1c). Recall that the failure trajectory is assumed to comprise a coordinated turn and a glide segment. If the glide segment has a distance of less than or equal to zero, the pie slice model is used instead (Fig.3), *i.e.*, the transition from the high altitude to low altitude model occurs when the glide component of the trajectory is zero, *i.e.*, $\boldsymbol{d_g = 0}$. The model illustrated in Fig.3. approximates the footprint for low altitudes using a circle sector (*e.g.,* pie slice) centred on the initial position $\boldsymbol{A}$ with radius equal to the maximum glide distance $\boldsymbol{d_{Max}}$. The pie slice half-angle $\boldsymbol{\theta}$, which through simple geometry, is half the turn angle. It is found that $\boldsymbol{\theta}$ can be estimated by setting $\boldsymbol{d_t}$ as an empirically determined factor of $\boldsymbol{d_{max}}$. Then, $\boldsymbol{d_t}$ and $\boldsymbol{r_t}$ can be used to determine $\boldsymbol{\phi}$ and hence $\boldsymbol{\theta}$. The resultant footprint area is:

$$A_{Pie\ Slice} = \theta d_{Max}^2 \quad (6)$$

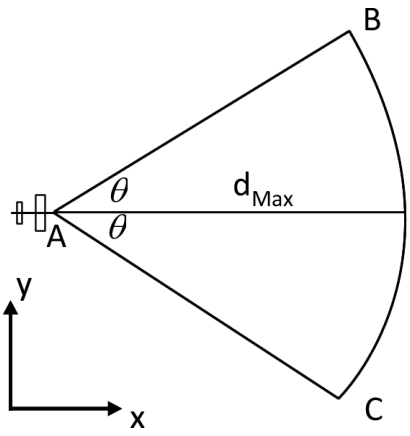

Figure 3. Pie Slice Geometric Approximation

3.4. Phase of Flight Footprint

The geometric templates described in §3.3 are for a single point in a flight plan. A mission can be described by a series of simplified phases, namely: cruise, loiter, climb and descent. By extrapolating the footprints and geometric footprint approximations derived in §3.3, it is possible to obtain the aggregate footprint for a given phase of flight. By combining the aggregated footprints for a series of phases it is then possible to construct the aggregate footprint for a mission. Note, that in the following equations $\boldsymbol{A_{Footprint}}$ refers to the footprint area as calculated using Eq.(**5**) or Eq.(**6**) depending on the initial height of the aircraft AGL.

3.4.1. Approximating the Impact Footprint for a Cruise Phases of Flight

Cruising flight is assumed to comprise straight and level flight at a constant height AGL. Thus, the aggregated footprint can be readily obtained by translating the footprint along the *x*-axis (*i.e.* along track axis) as shown in Fig.4. It can be seen that the two parameters needed to determine the aggregated footprint are the height AGL ***H*** and the cruise distance ***d*** (which can be derived from the assumed constant velocity and time spent in this phase). The aggregated footprint area can be approximated using:

$$A_{Cruise} = 2b_1 d + A_{Footprint} \tag{7}$$

where, b_1 is the maximum across track displacement and $A_{Footprint}$ is the footprint area (at a single instance in time). This approximation model is empirically verified for the Cessna 172 and Aerosonde aircraft against the 6DoF simulation. The relative error in the footprint area and Maximum Across Track Distance b_1 between the geometric template model and the 6DoF simulation are shown in Table 1. The average computation time is just 0.0159s on an Intel Core 2.66GHz mobile CPU. From Table 1, it can be seen that the relative error between the results computed using the geometric primitive and the results computed using the 6DoF simulation are very small, typically less than 1% for initial heights of 1000ft AGL.

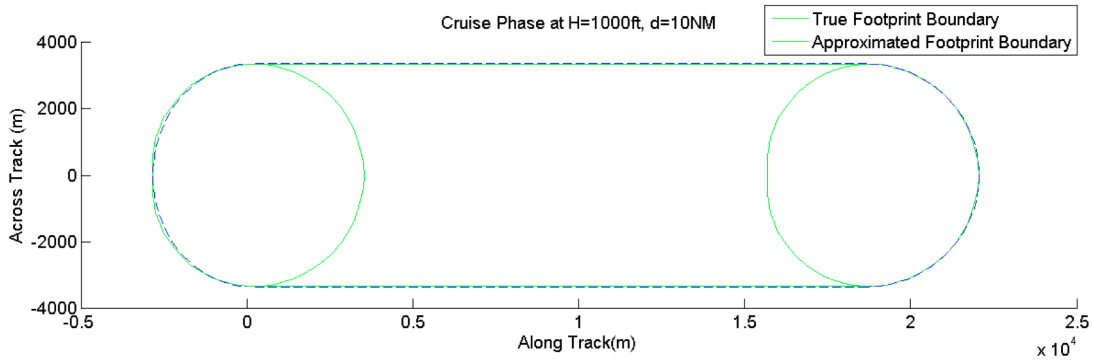

Figure 6. Aggregated Impact Footprint for a Cruise Phase of Flight (H = 1000ft, d = 10NM).

Table 1. Relative Error in the Aggregated Footprint Area and Maximum Across Track Distance For Cruise Flight (Comparison Between Geometric Model and 6DoF Simulation)

	Cessna 172 H			**Aerosonde H**		
d	**100ft**	**1000ft**	**5000ft**	**100ft**	**1000ft**	**5000ft**
10NM	5.2%	0.07%	0.41%	0.24%	0.22%	0.40%
50NM	5.2%	0.21%	0.32%	0.18%	0.20%	0.29%
100NM	5.2%	0.24%	0.30%	0.17%	0.19%	0.24%
1000NM	5.2%	0.26%	0.27%	0.16%	0.18%	0.19%
b_1 relative error	5.2%	0.26%	0.27%	0.16%	0.18%	0.18%

3.4.2. Approximating the Impact Footprint for a Loiter Phase of Flight

A loiter is assumed to consist of a circular track of radius ***R*** at constant height AGL. The aggregated footprint is then found by translating and rotating the footprint along the circular track. This creates an annulus shaped aggregated footprint, which is a function of the footprint across-track "width" as shown in Fig.7. The footprint area is calculated using Eq.(**8**). This approximation method is empirically verified against the outputs from the 6DoF model (Table 2). The average computation time is 0.01s.

$$A_{Loiter} = \begin{cases} \pi(R + b_1)^2 & R < 2b_1 \\ \pi((R + b_1)^2 - \pi(R - b_1)^2) & R \geq 2b_1 \end{cases} \tag{8}$$

From Table 2, it can be seen that the relative error between the results computed using the geometric primitive and the results computed using the 6DoF simulation are very small. The error grows with decreasing altitude (typically $\boldsymbol{H}$ < 500ft AGL). This is due to the increasing relative error between the approximation provided by the high altitude footprint model and the 6DoF model as $\boldsymbol{H}$ tends to zero.

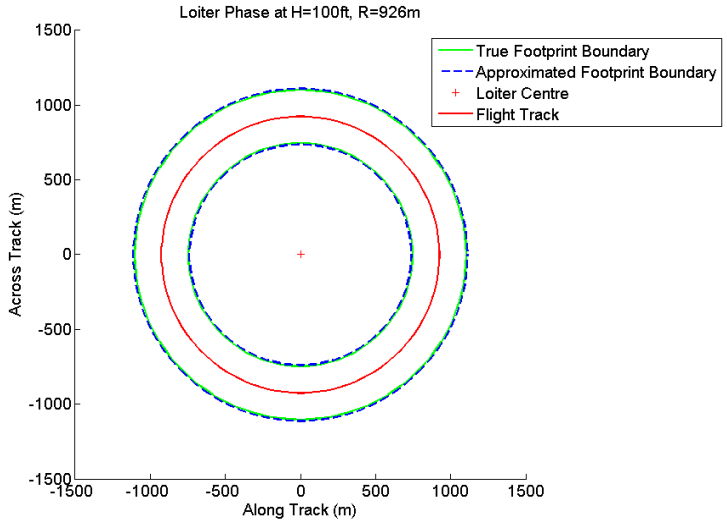

Figure 7. Example Aggregated Impact Footprint for a Loiter Phase

Table 2. Relative Error in the Aggregated Footprint Area and Maximum Across Track Distance For Loiter Flight (Comparison Between Geometric Model and 6DoF Simulation)

	Cessna 172 H			Aerosonde H		
R	**100ft**	**1000ft**	**5000ft**	**100ft**	**1000ft**	**5000ft**
0.1NM	5.2%	0.49%	0.53%	0.24%	0.36%	0.36%
0.5NM	5.2%	0.41%	0.51%	0.12%	0.32%	0.35%
1NM	5.2%	0.33%	0.49%	0.16%	0.28%	0.34%
5NM	5.2%	0.26%	0.35%	0.16%	0.15%	0.28%
b_1 relative error	5.2%	0.26%	0.27%	0.16%	0.18%	0.18%

3.4.3. Approximating the Impact Footprint for a Climb or Descent

In modelling the aggregated footprint area for a climb or descent phase of flight, it is assumed that the aircraft climbs/descends at a constant rate and in a straight line. Unlike the cruise and loiter phases, the shape and size of the footprint changes as the aircraft changes altitude.

The parameters used to characterise a climb/descent consist of the initial height AGL $\boldsymbol{H_1}$, the final height $\boldsymbol{H_2}$, and the distance $\boldsymbol{d}$ over which the climb occurs. By tracing the outermost boundary of the union of all individual footprints $\boldsymbol{A_i}$, it is possible to find the overall footprint. This is shown in Fig.8. and Eq.9. The geometric approximation model is again empirically verified against the results obtained from the 6DoF simulation (Table 3). The union of footprints takes more time to compute, approximately 0.28s on average.

$$A_{Climb\ or\ Descend} = F\left(\bigcup_{i=1\ldots N} A_i\right) \tag{9}$$

Again, it can be seen that the relative error between the results computed using the geometric primitive and the results computed using the 6DoF simulation are very small (Table 3). The results presented in Table 3 show that the aggregated geometric primitive provides a good approximation to the results generated by the computationally more expensive 6DoF simulation.

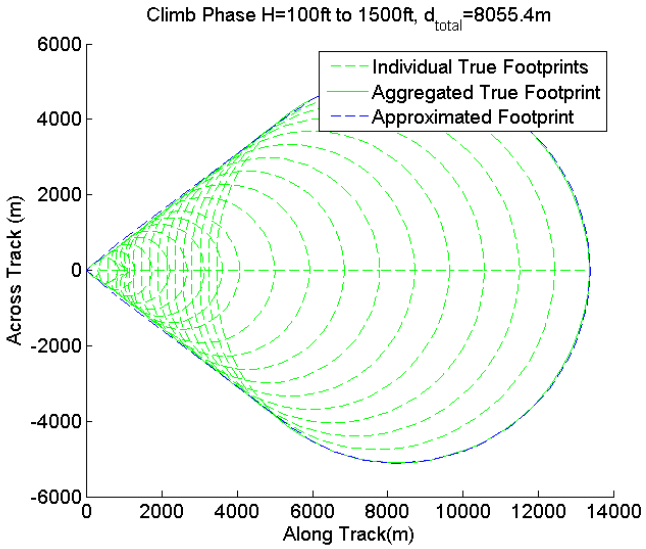

Figure 8. Example Aggregated Impact Distribution for a Climb Phase

Table 3. Relative Error in the Aggregated Footprint Area and Maximum Across Track Distance For a Climb/Descent (Comparison Between Geometric Model and 6DoF Simulation)

	Cessna 172 d			Aerosonde d		
H	**8055m**	**4985m**	**3198m**	**8055m**	**4985m**	**3198m**
100ft to 1500ft	0.57%	0.18%	0.24%	0.31%	0.31%	0.31%
1500ft to 4500ft	0.42%	0.42%	0.42%	0.42%	0.42%	0.42%
4500ft to 1500ft	0.42%	0.42%	0.42%	0.42%	0.42%	0.42%
1500ft to 100ft	0.28%	0.25%	0.24%	0.31%	0.31%	0.31%

3.4 Summary

This section has described the development of geometric templates/primitives that can be used to approximate the maximum boundary and area of the distribution of possible ground impact locations for a fixed wing aircraft. As shown by the example scenarios, the results obtained from the geometric templates have a low relative error when compared to the results calculated using a 6DoF model. The footprints can be extrapolated to describe a range of flight phases and missions with computation times of less than a second.

4. CONCLUSION

Assessments of the risk to people on the ground are a key input to the development of airworthiness regulations for UAS. These assessments should include measures of the CR, IR and SR. A review of the commonly used measure of CR, IR and SR was provided. Based on the review, it was determined that the model must be capable of describing the distribution of possible impact locations, given a failure at a particular point in the flight plan. Existing models either do not take the impact distribution into consideration, or propose computationally expensive methods for its calculation. A computationally efficient approach for estimating the boundary (and in turn area) of the impact distribution for fixed wing UA was proposed. A series of geometric templates that approximate the impact distributions are derived using an empirical analysis of the results obtained from a 6DoF simulation. The impact distributions can be aggregated to provide impact footprint distributions for a range of generic phases of flight and missions. The maximum footprint areas obtained from the geometric template model are shown to have a relative error of typically less than 1% compared to the areas calculated using the computationally more expensive 6DoF simulation. Computation times for the geometric models are on the order of one second or less, using a standard desktop computer. Future work includes characterising the distribution of impact locations within the template impact footprints.

Acknowledgements

Components of this work were completed as part of the UAS Risk Assessment Tool (URAT) Project; a project sponsored by the Defence Science and Technology Organisation (DSTO), Australian Government, Department of Defence. The URAT Project is detailed in the report: "Wu, P and Clothier R. ARCAA-URAT-RM-MD-001, UAS Risk Assessment Tool Project: Risk Model Derivation. Australian Research Centre for Aerospace Automation (ARCAA). Brisbane, Australia. 14 April 2011".

References

[1] Clothier, R A and Walker, R A. The Safety Risk Management of Unmanned Aircraft Systems. To appear in the Handbook of Unmanned Aerial Vehicles, K. P. Valavanis and G. J. Vachtsevanos, Eds., Dordrecht, Netherlands: Springer Science + Business Media B.V., 2012 (In press).

[2] JAA/EUROCONTROL. Final Report A Concept For European Regulations For Civil Unmanned Aerial Vehicles (UAVs). The Joint JAA/EUROCONTROL Initiative on UAVs, 11 May 2004.

[3] ISO. ISO 31000:2009, Risk management - Principles and guidelines. International Organization for Standardization (ISO), Switzerland, 2009.

[4] Clothier, R A, Palmer, J L, Walker, R A, and Fulton, N L. Definition of an Airworthiness Certification Framework for Civil Unmanned Aircraft Systems. Safety Science, vol. 49, pp. 871-885, 2011.

[5] Weibel, R and Hansman, R. Safety Considerations for Operation of Different Classes of UAVs in the NAS. In American Institute of Aeronautics and Astronautics, 3rd "Unmanned Unlimited" Technical Conference, Workshop and Exhibit, Chicago, Illinois, 2004.

[6] Clothier, R A, Walker, R A, Fulton, N L, and Campbell, D A. A Casualty Risk Analysis For Unmanned Aerial System (UAS) Operations Over Inhabited Areas. Presented at the Twelfth Australian International Aerospace Congress (AIAC-12), 2nd Australasian Unmanned Air Vehicles Conference, Melbourne, Australia, 2007.

[7] King, D W, Bertapelle, A, and Moses, C. UAV Failure Rate Criteria for Equivalent Level of Safety. Presented at the International Helicopter Safety Symposium, Montréal, Québec, Canada, 2005.

[8] Dalamagkidis, K, Valavanis, K P, and Piegl, L A. Evaluating the Risk of Unmanned AIrcraft Ground Impacts. Presented at the 16th Mediterranean Conference on Control and Automation, Ajaccio, France, 2008.

[9] McGeer, T, Newcome, L, and Vagners, J. Quantitative Risk Management as a Regulatory Approach to Civil UAVs. Presented at the International Workshop on UAV Certification, Paris, France, 1999.

[10] RCC. Standard 323-99, Range Safety Criteria for Unmanned Air Vehicles. Range Safety Group, Range Commanders Council, White Sands, New Mexico, 1999.

[11] RCC. Standard 323-99, Range Safety Criteria for Unmanned Air Vehicles, Rationale and Methodology Supplement. Range Safety Group, Range Commanders Council, White Sands, New Mexico, April 2001.

[12] Grimsley, F. Equivalent Safety Analysis Using Casualty Expectation Approach. In AIAA 3rd "Unmanned Unlimited" Technical Conference, Workshop and Exhibit, Chicago, Illinois, 2004.

[13] Thompson, K M. Variability and Uncertainty Meet Risk Management and Risk Communication. Risk Analysis, vol. 22, pp. 647-654, 2002.

[14] Thompson, K M, Rabouw, R F, and Cooke, R M. The Risk of Groundling Fatalities from Unintentional Airplane Crashes. Risk Analysis, vol. 21, pp. 1025-1037, 2001.

[15] Goldstein, B L, Demak, M, Northridge, M, and Wartenberg, D. Risk to Groundlings of Death due to Airplane Accidents: A Risk Communication Tool. Risk Analysis, vol. 12, pp. 339-341, 1992.

[16] Kostikov, V A, Smol'nikov, V L, Baranaev, Y D, Viktorov, A N, Vladykov, G M, Dolgov, V V, and Shvedenko, I M. Determination of the Probability of an Aircraft Falling on a Nuclear Power Plant. Atomic Energy, vol. 74, pp. 55-58, January 1993.

[17] Ale, B J M, Bellamy, L J, Cooke, R M, Goossens, L H J, Hale, A R, Roelen, A L C, and Smith, E. Towards a Causal Model for Air Transport Safety - An Ongoing Research Project. Safety Science, vol. 44, pp. 657-673, October 2006.

[18] Ale, B J M, Bellamy, L J, van der Boom, R, Cooper, J, Cooke, R M, Goossens, L H J, Hale, A R, Kurowicka, D, Morales, O, Roelen, A L C, and Spouge, J. Further Development of a Causal Model

for Air Transport Safety (CATS): Building the Mathematical Heart. Reliability and System Safety, vol. 94, pp. 1433-1441, September 2009.

[19] Ale, B J M and Piers, M. The Assessment and Management of Third Party Risk Around a Major Airport. Journal of Hazardous Materials, vol. 71, pp. 1-16, 2000.

[20] Evans, A W, Foot, P B, Mason, S M, Parker, I G, and Slater, K. R&D Report 9636, Third Party Risk Near Airports and Public Safety Zone Policy. National Air Traffic Services Limited, Department of the Environment, Transport and the Regions (DETR), London, UK, June 1997.

[21] Lin, M, Larson, E, and Collins, J. Volume II, Appendix D.16, Determination of Debris Risk to the Public Due to the Columbia Breakup During Reentry. ACTA, September 2003.

[22] Fulton, N and Robinson, G. Benchmark Public Risk Levels for Australian Space Launch Activities. Commonwealth Scientific and Industrial Research Organisation (CSIRO), Mathematical and Information Sciences, Canberra, Australia, July 2000.

[23] FAA. Advisory Circular, AC431.35-1, Expected Casualty Calculations For Commercial Space Launch And Reentry Missions. Federal Aviation Administration (FAA), Department of Transportation, Washington, DC, August 2000.

[24] RCC. Standard 321-02, Common Risk Criteria for National Test Ranges: Inert Debris. Range Safety Group Risk Committee, Range Commanders Council, US Army White Sands Missile Range, New Mexico, June 2002.

[25] Fulton, N L, Westcott, M, and Emery, S. Decision Support for Risk Assessment of Mid-air Collisions via Population-based Measures. Transportation Research Part A: Policy and Practice, vol. 43, pp. 150-169, February 2009.

[26] CCPS. Guidelines for Developing Quantitative Safety Risk Criteria Center for Chemical Process Safety (CCPS), John Wiley & Sons, Inc, Hoboken, 2009.

[27] Fulton, N L. Regional Airspace Design: A Structured Systems Engineering Approach. PhD, School of Aerospace and Mechanical Engineering, The University of New South Wales, Australian Defence Force Academy, Canberra, Australia, 2002.

[28] RCC. Standard 321-10, Common Risk Criteria For National Test Ranges. Range Safety Group Risk Committee, Range Commanders Council, US Army White Sands Missile Range, New Mexico, December 2010.

[29] Wiklund, E. Flying with Unmanned Aircraft (UAVs) in Airspace Involving Civil Aviation Activity Air Safety and the Approvals Procedure (English translation of "Flygning med obemannade luftfartyg (UAV) iluftrum med civil flygverksamhet"). The Swedish Aviation Safety Authority, Norrköping, Sweden, 2003.

[30] Clothier, R A, Palmer, J L, Walker, R A, and Fulton, N L. Definition of Airworthiness Categories for Civil Unmanned Aircraft Systems (UAS). Presented at the 27th International Congress of the Aeronautical Sciences, Nice, France, 2010.

[31] Fraser, C and Donnithorne-Tait, D. An Approach to the Classification of Unmanned Aircraft. In Bristol International Unmanned Aerial Vehicle Systems (UAVS) Conference, Bristol, UK, 2011, pp. 157-211.

[32] Magister, T. The Small Unmanned Aircraft Blunt Criterion Based Injury Potential Estimation. Safety Science, vol. 48, pp. 1313-1320, December 2010.

[33] Jones, D A. Nomenclature for Hazard and Risk Assessment in the Process Industries. 2nd ed. Institution of Chemical Engineers (IChemE), Rugby, 1992.

[34] Jonkman, S N, van Gelder, P H A J M, and Vrijling, J K. An Overview of Quantitative Risk Measures for Loss of Life and Economic Damage. Journal of Hazardous Materials, vol. 99, pp. 1-30, April 2003.

[35] Bottelberghs, P H. Risk Analysis and Safety Policy Developments in the Netherlands. Journal of Hazardous Materials, vol. 71, pp. 59-84, January 2000.

[36] Stallen, P J M, Geerts, R, and Vrijling, H K. Three Conceptions of Quantified Societal Risk. Risk Analysis, vol. 16, pp. 635-644, 1996.

[37] Pasman, H J and Vrijling, J K. Social Risk Assessment of Large Technical Systems. Human Factors and Ergonomics in Manufacturing & Service Industries, vol. 13, pp. 305-316, 2003.

[38] Laheij, G M H, Post, G J, and Ale, B J M. Standard Methods for Land-use Planning to Determine the Effects on Societal Risk. Journal of Hazardous Materials, vol. 71, pp. 269-282, January 2000.

[39] Piers, M. Methods and Models for the Assessment of Third Party Risk due to Aircraft Accidents in the Vicinity of Airports and their Implications for Societal Risk. In Quantified Societal Risk and

Policy Making, R. E. Jorissen and P. J. M. Stallen, Eds., Dordrecht: Kluwer Academic Publishers, 1998.

[40] Horn, M E T, Fulton, N, and Westcott, M. Measures of Societal Risk and Their Potential Use in Civil Aviation. Risk Analysis, vol. 28, pp. 1711-1726, 2008.

[41] RCC. Standard 321-07, Common Risk Criteria For National Test Ranges. Range Safety Group Risk Committee, Range Commanders Council, US Army White Sands Missile Range, New Mexico, June 2007.

[42] Evans, A W and Verlander, N Q. What is Wrong with Criterion FN-Lines for Judging the Tolerability of Risk? Risk Analysis, vol. 17, pp. 157-168, 1997.

[43] Farmer, F R. Reactor Safety and Siting: A Proposed Risk Criterion. Nuclear Safety, vol. 8, pp. 539-548, 1967.

[44] Wu, P and Clothier, R A. Development of Impact Footprints for the Analysis of UAS Risks Over Inhabited Areas. Internal Report for DSTO URAT Project. Australian Research Centre for Aerospace Automation, Queensland University of Technology, Brisbane, April 2011.